Available online at www.sciencedirect.com

SciVerse ScienceDirect

Energy Procedia 31 (2012) 60 – 68

Energy Procedia

E-MRS Spring Meeting 2011, Symposium S: Organic Photovoltaics: Science and Technology

The influence of substrate and top electrode on the crystallization dynamics of P3HT:PCBM blends

Samuele Lilliu[a*], Tiziano Agostinelli[b], Mark Hampton[a], Ellis Pires[a], Jenny Nelson[b], J. Emyr Macdonald[a]

[a]*School of Physics and Astronomy, Cardiff University, Queens Buildings, The Parade, Cardiff CF243AA, United Kingdom*
[b] *Department of Physics and Centre for Plastic Electronics, Blackett Laboratory, Imperial College London, Prince Consort Road, London SW7 2BW, United Kingdom*

Abstract

Substrate and top electrode effects on P3HT lamellar crystallization, were studied using the full device structure of a bulk-hetorojunction P3HT:PCBM organic solar cell, during thermal annealing. P3HT: PCBM chlorobenzene solutions (50 wt %) were spin coated on quartz, HMDS treated SiO_2, SiO_2/ PEDOT: PSS, ITO/ PEDOT: PSS. The structural evolution of these thick (~100nm) films was probed during a realistic device-processing annealing cycle at 140ºC for ~53 minutes by time-resolved synchrotron Grazing Incidence X-Ray Diffraction (GI-XRD). The 20 nm-thick coated Aluminium layer on top of ITO/ PEDOT: PSS/ P3HT: PCBM acts as a nucleation site for the P3HT crystalline growth during annealing, increasing the number of the edge-on lamellae, and preferentially increasing the domain size of face on and edge-on lamellae, with minor growth of the randomly oriented lamellae.

Keywords: Crystallization; Thin Film; P3HT: PCBM; Grazing Incidence X-Ray Diffraction

1. Introduction

Poly-(3-hexyl)thiophene (P3HT) and [6-6-]-phenyl-C_{61}-butyric acid methyl ester (PCBM) is the most widely studied material system for bulk heterojunction (BHJ) organic photovoltaic devices, with reported power conversion efficiencies (PCE) of 4-5%. [1-4] Further studies on the optimization of BHJ films based on P3HT: PCBM could help to find quick optimization routes for new materials systems. In-situ

* Corresponding author. *E-mail address:* samuele_lilliu@hotmail.it

doi:10.1016/j.egypro.2012.11.165

grazing incidence X-ray diffraction (GIXRD) has recently contributed to a wider understanding of crystallization phenomena, during the drying process after the film deposition and during (thermal and solvent) annealing. [1, 5-13] Since the crystallization dynamics is a fast process, the capability of probing diffraction images at high rates is required to follow the process in real time. [6, 7] The analysis of P3HT crystallization as a function of the drying/annealing time, as well as the study of its lamellar packing, are currently helping to attain a wider understanding on how OPV performances are influenced by drying and annealing processes.

In-situ GI-XRD and ellipsometry were employed to study the self-organization in P3HT: PCBM blends in real-time, capturing diffraction images every 50 ms, during the drying process after in-situ doctor blading. [9] Following a similar approach, an X-ray investigation of the composition dependence on the structural evolution (crystallization dynamics and lamellar orientation) during drying of doctor bladed blends of P3HT: PCBM, where images were collected with a sampling time of 50 s, recently appeared in literature. [14] A real-time GI-XRD analysis of P3HT: PCBM films (spin-coated from chlorobenzene on SiO_2) during annealing (at 140°C), detailing the concentration effects on the crystallization dynamics, disorder and P3HT orientational spread, was conducted with a sampling time of 8s. [6] These results, coupled with ellipsometry and FET measurements, showed a link between the increase in P3HT crystallization during annealing and the enhancement in the PCE. [7] The in-situ morphology and OPV device data changes upon thermal annealing (at 140°C) in BHJ films of P3HT: PCBM (spin-coated from chlorobenzene on ITO/PEDOT: PSS) were studied by Shin et al. using a sampling time higher than 2 min. [15] The same study, using two different annealing temperature (150°C and 160°C), was subsequently performed by Nam et al. [16]

Detailed time-resolved GI-XRD during annealing of P3HT: PCBM full and partial device structure, coupled with a comparison between different substrates, has not been published to date. In this work, using synchrotron GI-XRD, we probe in-situ changes of crystalline structures in P3HT: PCBM (1:1 w/w) blends during thermal annealing at a fixed temperature (140 °C). The following samples have been analyzed: P3HT:PCBM spin-coated on PEDOT: PSS/ ITO substrates (with and without a top Al electrode); P3HT:PCBM spin-coated on quartz, SiO_2/HMDS, and SiO_2/PEDOT:PSS substrates.

2. Experimental

2.1. Samples Preparation

Different substrates were employed in this study: transparent indium-tin-oxide (ITO) coated glass (Visiontek Systems), 1 mm thick silicon with a 300 nm oxide layer (IDB Technologies), and 2 mm thick quartz (Spectrosil B fused-silica, Kaypul Optics Limited) substrate. All the substrates, having an approximate size of 1×1 cm², were sequentially cleaned in acetone and isopropanol for 15 minutes each, rinsed with deionized water, and dried with a nitrogen gun. A low conductivity poly(3,4-ethylenedioxythiophene) poly(styrenesulfonate) (PEDOT:PSS, Clevios P standard grade, HC stark) aqueous solution was spin-coated onto ITO and SiO_2), substrates which were subsequently annealed at 200 °C for 30 minutes, resulting in a thickness of ~50 nm (on PEDOT:PSS) and ~65 nm (on SiO_2). Other SiO_2 substrates were pre-coated with hydrophobic self-assembled hexamethyldisilazane monolayer (HMDS). A regioregular poly(3-hexylthiophene) (rr-P3HT, with M_n = 19.5 KD, M_w = 34.1 KD, polydispersity index = 1.74, and regioregularity 94.7%, Merck Chemicals) and [6,6]-phenyl C61 butyric acid methyl ester (PCBM, Solenne BV) solution (50 wt % P3HT) was prepared in a glove box with chlorobenzene (30 mg/mL), and spin-coated in ambient conditions onto the quartz, SiO_2/HMDS, SiO_2/PEDOT:PSS, ITO/ PEDOT:PSS samples. The thicknesses were ~270 nm (on ITO/ PEDOT:PSS and SiO_2/PEDOT:PSS), ~100 nm (on SiO_2), ~190 nm (SiO_2/HMDS), ~345 nm (on quartz). About 20 nm of

aluminium were evaporated onto some of the ITO/ PEDOT:PSS/P3HT:PCBM samples using an evaporator enclosed in the glove box.

2.2. Grazing Incidence X-Ray Diffraction

GI-XRD measurements were performed at the XMaS beamline (BM28, ESRF, Grenoble, France) using a home-built chamber. Details on the Grazing Incidence Wide Angle X-Ray Scattering (GI-WAXS) geometry and setup have already been reported. [6, 7] The Out-OfPlane (OOP) incident angle α_i was set above the critical angle (α_c + 0.25°) for all the scans. The sample temperature was increased up to 140°C in ~2 minutes using automated PID temperature control. The overshoot was 5 °C and stabilized to 140±0.5°C after 4 minutes. The annealing lasted ~53 minutes, for a total of ~180 images. After annealing, the temperature controller was switched off and the sample cooled down. The sample took 4.5 minutes to reach <35 °C. Details on the software (GI-XRD-GUI), built for the Grazing Incidence X-ray diffraction images analysis, the calibration procedure, required to convert an image pixel coordinate into its corresponding scattering vector q, and the analysis can be found in Lilliu et al. [6]

In-Plane (IP) line profiles (image quasi-polar angle β = 75°, integration aperture $\Delta\beta$ = 10°), OOP line profiles ($\Delta\beta$ = 10°, β = 0°), and line profiles with β = 15, 30, 45, 60° were extracted for all the scans (here the term 'line profile' is used as a synonym for 'cake slice'). A procedure for a batch adaptive background subtraction via cubic splines and peak detection was implemented in the GI-XRD-GUI. Three significant parameters were extracted from each peak: (i) FWHM, (ii) peak center, (iii) peak integral. The FWHM contains information about the domain size, the peak center contains information about the d-spacing (lattice constant), and the peak integral (from FWHM and intensity) contains information about the number of crystallites. [6]

3. Results and Discussion

3.1. Diffraction Patterns

Prior to GIXRD measurements on the P3HT: PCBM films, glass/ITO substrates with and without PEDOT:PSS, and PEDOT:PSS on SiO_2 were examined (**Figure 1**). **Figure 1a** shows the ITO diffraction pattern. The sharp peak results from the superposition of two peaks around q = 1.51 Å^{-1} and q = 1.54 Å^{-1} and can be attributed to ITO, while the broad peak at q = 1.63 Å^{-1} can be assigned to glass. [15] In the case of PEDOT:PSS on SiO_2 (**Figure 1b**) two broad amorphous rings at q = 0.40 Å^{-1} and q = 1.28 Å^{-1} were detected. The diffraction pattern of PEDOT:PSS on ITO (**Figure 1c, 1d**) is simply the superimposition of the one from ITO and the one from PEDOT:PSS on SiO_2. The PEDOT:PSS diffraction pattern here observed is isotropic. The anisotropy reported in Shin et al. could be due to the strong signal coming from the reflected beam, which affects any OOP line profile, independently from the film composition. [15]

After clarifying the diffraction patterns from the PEDOT:PSS layer and the glass/ITO substrate, we performed time-resolved GIXRD, collecting images every ~18 seconds. A sampling time higher than 2 minutes would not be enough to draw conclusion on the crystallization dynamics, since most of the changes in the P3HT: PCBM film occur within the first 3-6 minutes of annealing. [6, 7] As in our previous works, here we index P3HT peaks using the same convention used by Kayunkid et al. [6, 7, 17] P3HT polymer backbones stack in the direction of the alkyl side chains (***a***-direction) forming a lamella. Adjacent lamellae stack (stacking distance = b/2) perpendicularly to the co-facial conjugated backbones (***b***-direction). The π-stacking direction is almost orthogonal to the alkyl-stacking direction in the unit cell, and can be parallel to the sample substrate, with the alkyl-stacking direction perpendicular (edge-on) to

the sample substrate, or with the alkyl-stacking direction parallel to the sample substrate (face-on). [6] In reality there are lamellae with intermediate orientations, i.e. with different angles between the substrate and the ***a*-**direction. [6]

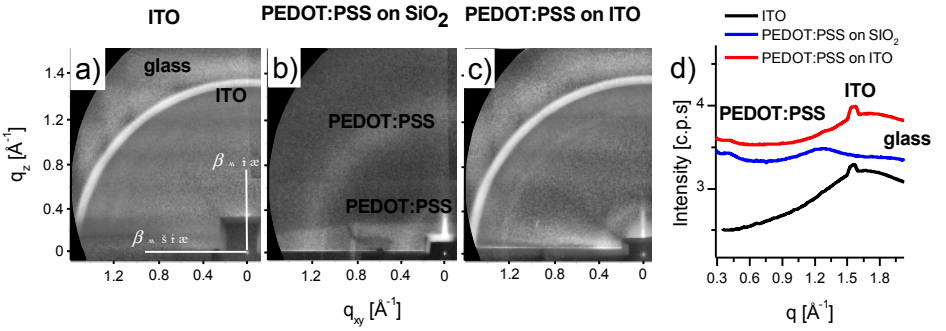

Fig. 1. ITO (a), PEDOT:PSS on SiO2 (b) and PEDOT:PSS on ITO (c) diffraction patterns. Line profiles (d). Diffraction patterns have been treated with an adaptive histogram equalization [5]. Lines profiles have been generated using $\beta = 15°$ to highlight the first PEDOT: PSS ring, which in a $\beta = 0°$ line profile would have been buried by the low-q scattering.

In the first set of experiments we focused on the top electrode effects on the film morphology and dynamics, studying device-like films with and without the top electrode. **Figure 2(a)-(d)** shows the diffraction patterns for ITO/PEDOT:PSS/P3HT:PCBM and ITO/PEDOT:PSS/P3HT:PCBM/Al, around the (100)-P3HT ring before and after the annealing. Line profiles are shown in **Figure 2(e)-(f)**. The (200) and (300)-P3HT peaks could not be clearly resolved for detailed fitting of line profiles for the samples coated on ITO. Moreover scattering from glass coincided with the scattering from the (020)-P3HT and PCBM. Scattering from PEDOT:PSS could not be observed, being too weak.

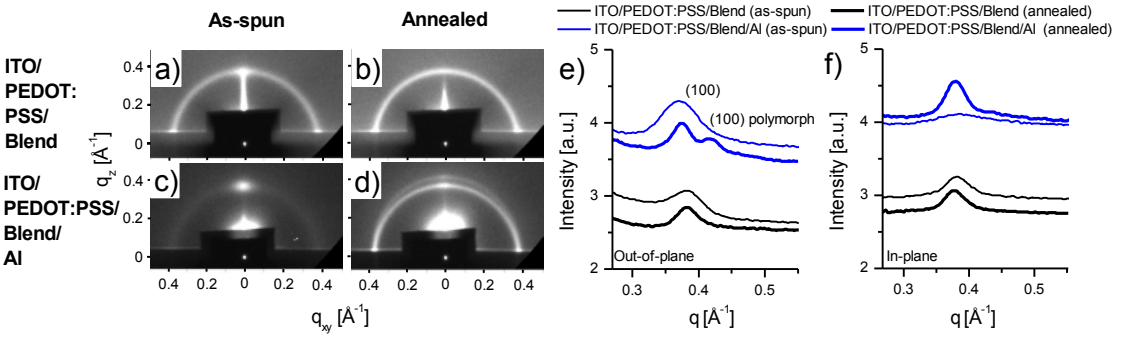

Fig. 2. ITO/PEDOT:PSS/Blend before (a) and after (b) annealing, ITO/PEDOT:PSS/Blend/Al before (c) and after (d) annealing. Out-Of-Plane (e) and In-Plane (f) line profiles around the (100)-P3HT peak, before and after annealing.

In the second set of experiments we focused on the substrate effects on the film morphology and dynamics. The same annealing procedure was followed for the processing of P3HT:PCBM spin-coated on quartz, SiO_2/HMDS, and SiO_2/PEDOT:PSS samples. The diffraction patterns, before and after annealing, around the (100)-P3HT peak, are shown in **Figure 3(a)-(h)**. The line profiles, before and after annealing,

are shown in **Figure 3 (g)-(h)**. In these cases the scattering from the substrate did not compromise the SNR of the higher order P3HT reflections, and the (*h*00)-P3HT peaks could be extracted and fitted.

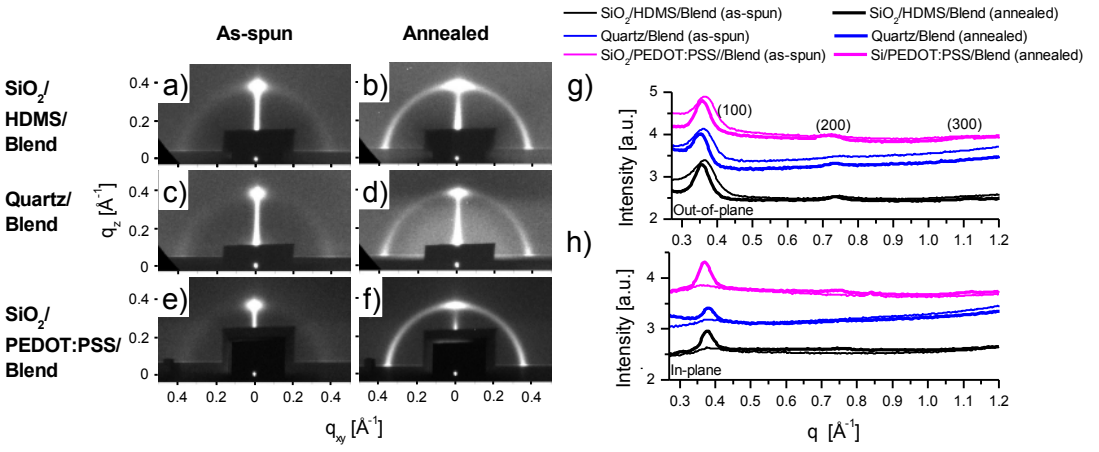

Fig. 3. iO2/HMDS/Blend before (a) and after (b) annealing, Quartz/Blend before (c) and after (d) annealing, SiO_2/PEDOT:PSS/Blend before (e) and after (f) annealing. Out-Of-Plane (g) and In-Plane (h) line profiles line profiles around the (*h*00)-P3HT peaks, before (thin lines) and after annealing (thick lines).

3.2. Crystallization Dynamics

Domain size dynamics can be tracked by monitoring the FWHM of the (100) peaks. **Figure 4(a)-(b)** shows the IP-(100) and OOP-(100) domain sizes calculated using the Scherrer equation, which usually overestimates the real domain size of ~1-2 nm. [6] Data extracted from the OOP-(*h*00)-P3HT refers to the edge-on lamellae, while data extracted from IP-(*h*00)-P3HS refers to the face-on lamellae. More accurate values using the Williamson-Hall (WH) approach, to quantify the degree of paracrystalline stacking disorder along the (100) direction, could not be calculated for the blends spin-coated ITO/PEDOT: PSS substrates because of the lack of higher order peaks (i.e. (200) and (300)). [6, 18-20] The use of more advanced techniques based on the Fourier analysis of the diffraction peaks was beyond the scope of the present work. All the samples show a similar crystallization trend, as already observed by Lilliu et al. for P3HT: PCBM films with different concentrations, spin-coated on SiO_2. [6] Crystallization occurs in the first 10 minutes of the annealing, reaching a value which does not significantly change during the rest of the annealing. However the sample spin-coated on quartz shows a slower dynamics in the IP-100-P3HT than the others: a continuous growth of the face-on lamellae is observed during the 53 min thermal treatment. At the end of the annealing, when the samples are cooled down, the domain sizes experience a slight reduction due to thermal contraction. [6] ITO/PEDOT:PSS/Blend/Al IP and OOP domain size values are both ~200 Å. This value is significantly higher than the values calculated for the other simples ranging between ~150 and ~175 Å (IP) and between ~158 and ~158 Å (OOP).

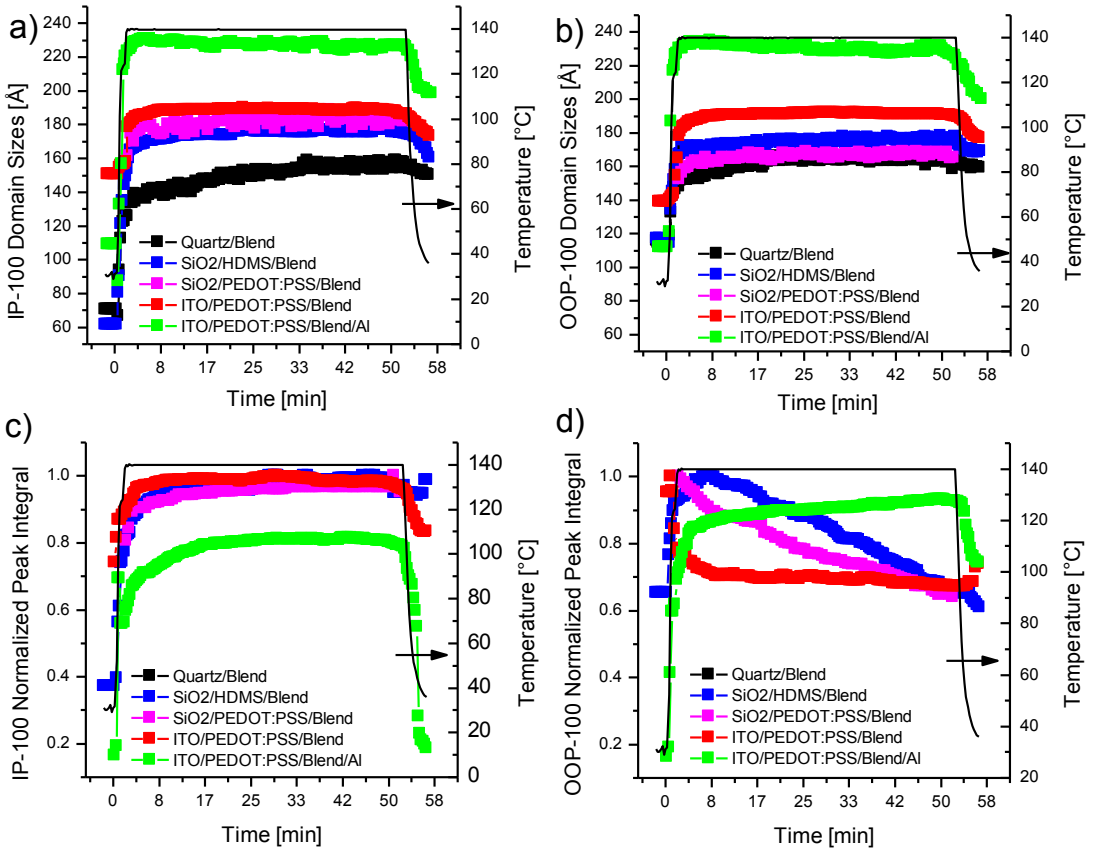

Fig. 4. IP-(100) domain sizes (a), OOP-(100) domain sizes (b), IP-(100) normalized peak integrals (c), OOP-(100) normalized peak integrals (d) as a function of the annealing time. The ordinate on the right shows the temperature.

Strong differences are observed between IP and OOP normalized peak integrals, which are proportional to the normalized amount of P3HT crystalline material. Whereas for all the IP peak integrals, increasing temperature gives an increase in the peak integral, for the OOP peak integrals, except for the ITO/PEDOT:PSS/(Blend)/Al, the behavior is reversed. This could correspond to a lamellar reorientation.

The average lattice constant, *a,* calculated from the (100)-P3HT peak position, varied from ~16.4 Å for the as-spun samples to ~17.4 Å in the first stages of the annealing. During the annealing the lattice constant experienced a reduction of about ~0.1 Å, and reduced to ~16.7 Å after cooling down, corresponding to an increase of ~0.3 Å with respect to the as-spun value. This permanent lattice constant increase has already been observed in previous reports. [6-8, 21]. Figure 4 – IP-(100) domain sizes (a), OOP-(100) domain sizes (b), IP-(100) normalized peak integrals (c), OOP-(100) normalized peak integrals (d) as a function of the annealing time. The ordinate on the right shows the temperature.

3.3. Lamellar Orientation

As shown in **Figure 2**, the presence of the top electrode strongly affects the P3HT lamellar packing. These differences can be quantified using radial profiles extracted at different β angles. As mentioned above, (100)-P3HT data extracted from the line profiles at $\beta = 0°$ (OOP-(*h*00)-P3HT) refers to the edge-

on lamellae, while data extracted at at β = 85° (IP-(*h*00)-P3HS) refers to the face-on lamellae. Line profiles with β between 60° and 15° contain information on lamellae with intermediate orientations.

Figure 5(a) summarizes the domain sizes and the (normalized) peak integral ('pole figure') extracted from the (100)-P3HT peaks, from line profiles taken at different β angles. [22] Both the as-spun ITO/PEDOT: PSS samples show a uniform distribution of the domain sizes. The annealed samples show larger domain sizes than the as-spun samples. While the domain sizes are uniformally distributed with angle β in the case of the annealed ITO/PEDOT: PSS sample without a top electrode, preferential growth in the IP and OOP lamellae is observed in the sample with the top electrode after annealing. The % variation of the domain size (**Figure 5(b))** is more pronounced for the full device structure (with Al).

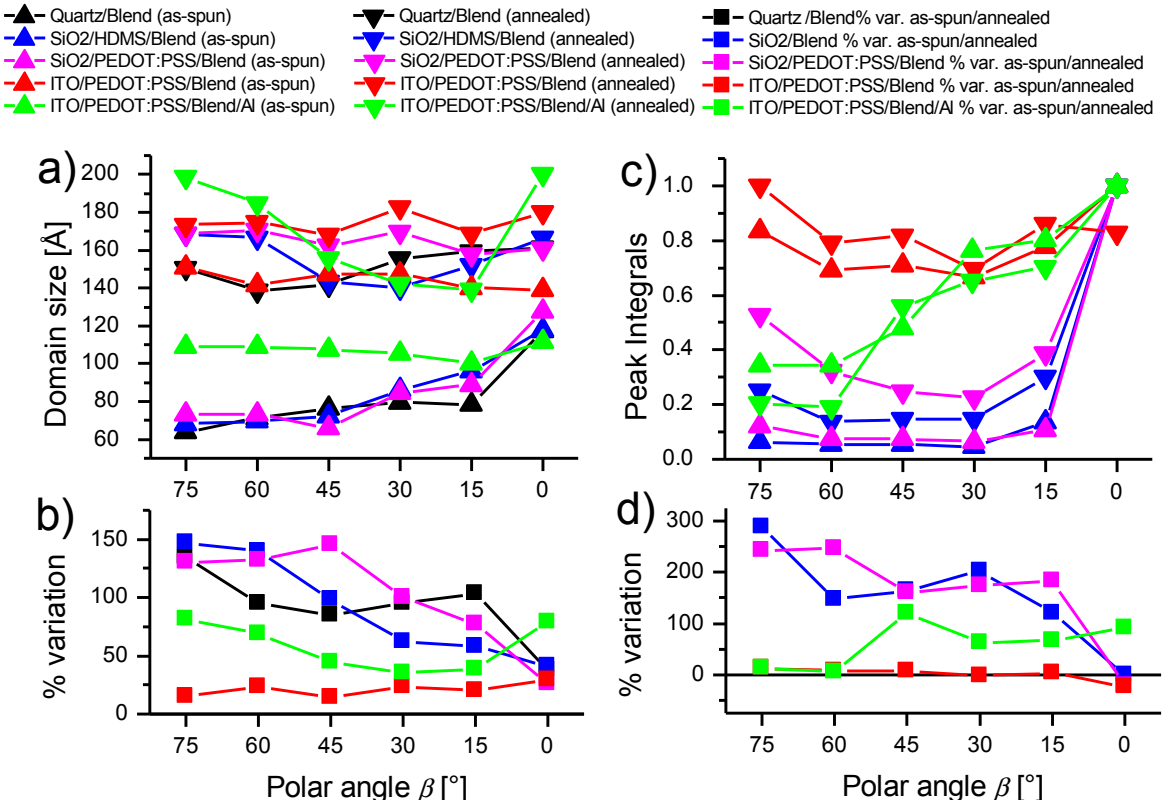

Fig. 5. Domain sizes before and after annealing (a) and their % variation (b), and normalized peak integrals before and after annealing (c) and their % variation (d), as a function of β. The variation is calculated as: ($Value_{annealed}$-$Value_{as\text{-}spun}$)/ $Value_{as\text{-}spun}$. For the ITO/PEDOT: PSS/Blend (annealed) domain size (a), the sharp variation between β = 0 and 15 and the less pronounced variation between β = 75 and 45 reflect the preferential growth in the IP and OOP lamellae.

Analogous curves are shown in **Figure 5(a)-(b)** for the remaining samples (SiO_2/HMDS, SiO_2/PEDOT:PSS, and quartz substrates) used to investigate the substrate effects on the P3HT lamellar packing. The distribution of domain size values monotonically increases from β = 75° (IP) to β = 0° (OOP) for the pristine samples. A significant growth of all the domain sizes, stronger for the IP lamellae,

is observed after the annealing. The distribution of the domain size values as a function of β is uniform after the annealing.

In the sample coated on ITO/PEDOT: PSS without a top Al electrode, slight growth of the number of IP P3HT crystallites, accompanied by a decrease of the OOP P3HT crystalline material, is observed after the annealing (**Figure 5(c)-(d)**). In the sample with the top electrode, similar IP growth is observed, but the OOP behavior is opposite to the other sample: apart from the outlier at $\beta = 45^{\circ}$, the number of OOP P3HT crystallites increases by ~90% after the annealing. Therefore the presence of Al, as the top electrode, seems to stimulate a preferential growth of the IP and OOP lamellae, as well as an increase of their number. Regarding the other samples a remarked increase in the number of the number of IP lamellae is accompanied by a slight reduction in the number of OOP lamellae.

4. Conclusions

We have shown a detailed comparison between crystallographic properties of semi-crystalline P3HT in P3HT: PCBM films deposited on different substrates and on ITO/ PEDOT: PSS substrates used in the preparation of real OPV devices (with and without Al electrode). Data was collected in real-time during the annealing procedure. The presence of the top electrode on the P3HT: PCBM film seems to enhance the nucleation of P3HT crystallites, favoring preferential growth of face and edge-on lamellae. No substantial differences where observed among films deposited on different substrates.

Acknowledgements

We thank the BM28 (XmaS, ESRF, Grenoble, France) team for help at the beamline. We would like to thank R. Tucker for help with the instrumentation. This work was partially funded by the Engineering and Physical Sciences Research Council (EPSRC) grant number EP/F016255, EP/F023200, EP/G031088, EP/F061757, EP/F056710, and Research Councils U.K. (RCUK). We acknowledge the Royal Society as well

References

[1] Y. Kim, S. Cook, S.M. Tuladhar, S.A. Choulis, J. Nelson, J.R. Durrant, D.D.C. Bradley, M. Giles, I. McCulloch, C.-S. Ha, M. Ree, A strong regioregularity effect in self-organizing conjugated polymer films and high-efficiency polythiophene:fullerene solar cells, Nat Mater, 5 (2006) 197-203.

[2] G. Li, V. Shrotriya, J. Huang, Y. Yao, T. Moriarty, K. Emery, Y. Yang, High-efficiency solution processable polymer photovoltaic cells by self-organization of polymer blends, Nat Mater, 4 (2005) 864-868.

[3] M.D. Irwin, D.B. Buchholz, A.W. Hains, R.P.H. Chang, T.J. Marks, p-Type semiconducting nickel oxide as an efficiency-enhancing anode interfacial layer in polymer bulk-heterojunction solar cells, Proceedings of the National Academy of Sciences, 105 (2008) 2783-2787.

[4] M. Wolff, A. Magerl, H. Zabel, Structure of polymer micelles at the solid interface, Physica B: Condensed Matter, 357 (2005) 84-87.

[5] J.H. Park, J.S. Kim, J.H. Lee, W.H. Lee, K. Cho, Effect of Annealing Solvent Solubility on the Performance of Poly(3-hexylthiophene)/Methanofullerene Solar Cells, The Journal of Physical Chemistry C, 113 (2009) 17579-17584.

[6] S. Lilliu, T. Agostinelli, E. Pires, M. Hampton, J. Nelson, J.E. Macdonald, Dynamics of Crystallization and Disorder during Annealing of P3HT/PCBM Bulk Heterojunctions, Macromolecules, 44 (2011) 2725-2734.

[7] T. Agostinelli, S. Lilliu, J.G. Labram, M. Campoy-Quiles, M. Hampton, E. Pires, J. Rawle, O. Bikondoa, D.D.C. Bradley, T.D. Anthopoulos, J. Nelson, J.E. Macdonald, Real-Time Investigation of Crystallization and Phase-Segregation Dynamics in P3HT:PCBM Solar Cells During Thermal Annealing, Advanced Functional Materials, 21 (2011) 1701–1708.

[8] E. Verploegen, R. Mondal, C.J. Bettinger, S. Sok, M.F. Toney, Z. Bao, Effects of Thermal Annealing Upon the Morphology of Polymer–Fullerene Blends, Advanced Functional Materials, 20 (2010) 3519-3529.

[9] T. Wang, A.D.F. Dunbar, P.A. Staniec, A.J. Pearson, P.E. Hopkinson, J.E. MacDonald, S. Lilliu, C. Pizzey, N.J. Terrill, A.M. Donald, A.J. Ryan, R.A.L. Jones, D.G. Lidzey, The development of nanoscale morphology in polymer:fullerene photovoltaic blends during solvent casting, Soft Matter, 6 (2010) 4128-4134.
[10] H.-Y. Chen, H. Yang, G. Yang, S. Sista, R. Zadoyan, G. Li, Y. Yang, Fast-Grown Interpenetrating Network in Poly(3-hexylthiophene): Methanofullerenes Solar Cells Processed with Additive, The Journal of Physical Chemistry C, 113 (2009) 7946-7953.
[11] T. Erb, U. Zhokhavets, G. Gobsch, S. Raleva, B. Stühn, P. Schilinsky, C. Waldauf, C.J. Brabec, Correlation Between Structural and Optical Properties of Composite Polymer/Fullerene Films for Organic Solar Cells, Advanced Functional Materials, 15 (2005) 1193-1196.
[12] C.-W. Chu, H. Yang, W.-J. Hou, J. Huang, G. Li, Y. Yang, Control of the nanoscale crystallinity and phase separation in polymer solar cells, Applied Physics Letters, 92 (2008) 103306-103303.
[13] N.D. Treat, M.A. Brady, G. Smith, M.F. Toney, E.J. Kramer, C.J. Hawker, M.L. Chabinyc, Interdiffusion of PCBM and P3HT Reveals Miscibility in a Photovoltaically Active Blend, Advanced Energy Materials, 1 (2011) 82-89.
[14] M. Sanyal, B. Schmidt-Hansberg, M.F.G. Klein, C. Munuera, A. Vorobiev, A. Colsmann, P. Scharfer, U. Lemmer, W. Schabel, H. Dosch, E. Barrena, Effect of Photovoltaic Polymer/Fullerene Blend Composition Ratio on Microstructure Evolution during Film Solidification Investigated in Real Time by X-ray Diffraction, Macromolecules, 44 (2011) 3795–3800.
[15] M. Shin, H. Kim, J. Park, S. Nam, K. Heo, M. Ree, C.-S. Ha, Y. Kim, Abrupt Morphology Change upon Thermal Annealing in Poly(3-Hexylthiophene)/Soluble Fullerene Blend Films for Polymer Solar Cells, Advanced Functional Materials, 20 748-754.
[16] S. Nam, M. Shin, H. Kim, Y. Kim, Temperature/time-dependent crystallization of polythiophene:fullerene bulk heterojunction films for polymer solar cells, Nanoscale, 2 (2010) 2384-2389.
[17] N. Kayunkid, S. Uttiya, M. Brinkmann, Structural Model of Regioregular Poly(3-hexylthiophene) Obtained by Electron Diffraction Analysis, Macromolecules, 43 (2010) 4961-4967.
[18] R. Hosemann, Röntgeninterferenzen an Stoffen mit flüssigkeitsstatistischen Gitterstörungen, ZEITSCHRIFT FÜR PHYSIK, 128 (1950) 465-492.
[19] R.H. Hosemann, A.M. , Structure of crystalline and paracrystalline condensed matter, J. Macromol. Sci. Phys., B34 (1995) 327-356.
[20] T.-M. Wu, J. Blackwell, S.N. Chvalun, Determination of the Axial Correlation Lengths and Paracrystalline Distortion for Aromatic Copolyimides of Random Monomer Sequence, Macromolecules, 28 (1995) 7349-7354.
[21] O. Werzer, K. Matoy, P. Strohriegl, R. Resel, Temperature treatment of semiconducting polymers: An X-ray reflectivity study, Thin Solid Films, 515 (2007) 5601-5605.
[22] J. Rivnay, R. Noriega, J.E. Northrup, R.J. Kline, M.F. Toney, A. Salleo, Structural origin of gap states in semicrystalline polymers and the implications for charge transport, Physical Review B, 83 (2011) 121306.